Sound field reconstruciton using a spherical microphone array.

Fernandez Grande, Efren

Published in:
Journal of the Acoustical Society of America

Link to article, DOI:
10.1121/1.4943545

Publication date:
2016

Document Version
Publisher's PDF, also known as Version of record

Sound field reconstruction using a spherical microphone array[a)]

Efren Fernandez-Grande[b)]
Acoustic Technology, Department of Electrical Engineering, Technical University of Denmark (DTU), Building 352, Ørsteds Plads, DK-2800 Kongens Lyngby, Denmark

(Received 17 February 2015; revised 2 February 2016; accepted 12 February 2016; published online 17 March 2016)

A method is presented that makes it possible to reconstruct an arbitrary sound field based on measurements with a spherical microphone array. The proposed method (spherical equivalent source method) makes use of a point source expansion to describe the sound field on the rigid spherical array, from which it is possible to reconstruct the sound field over a three-dimensional domain, inferring all acoustic quantities: sound pressure, particle velocity, and sound intensity. The problem is formulated using a Neumann Green's function that accounts for the presence of the rigid sphere in the medium. One can reconstruct the total sound field, or only the incident part, i.e., the scattering introduced by the sphere can be removed, making the array virtually transparent. The method makes it possible to use sequential measurements: different measurement positions can be combined, providing an extended measurement area consisting of an array of spheres, and the sound field at any point of the source-free domain can be estimated, not being restricted to spherical surfaces. Because it is formulated as an elementary wave model, it allows for diverse solution strategies (least squares, ℓ_1-norm minimization, etc.), revealing an interesting perspective for further work.
 [http://dx.doi.org/10.1121/1.4943545]

[EGW] Pages: 1168–1178

I. INTRODUCTION

Microphone array processing is essential for characterizing complex sound fields and for studying how acoustic sources radiate sound. Planar arrays are generally the most used configuration, although it is far from being the only one. Uniform linear arrays, circular,[1–3] cylindrical,[4] and spherical arrays[5–7] are commonly found, as well as several other configurations.[8,9]

Spherical microphone arrays are particularly well suited for applications where sound waves impinge on the array from multiple directions, such as enclosures and non-anechoic spaces, or cases where multiple sources around the array may exist. They make it possible to resolve waves traveling in any direction, whereas this is not necessarily the case for conventional planar arrays.[10,11] Spherical microphone arrays are widely used for sound source localization,[12–14] sound field reproduction—to capture sound fields that can be reproduced with an array of loudspeakers,[15–18] and sound field analysis and reconstruction.[19–26]

The use of rigid spherical microphone arrays for reconstructing sound fields has been the subject of several studies,[20–24] which employ a spherical harmonic expansion to provide a full representation of the sound field (sound pressure, particle velocity, and sound intensity). The expansion is used to extrapolate the sound field to a different radius than measured, thus reconstructing the sound field over a three-dimensional space about the array, i.e., predicting the sound field elsewhere than measured. These studies have aimed at reconstructing either the total sound field[20,24] or only the incident waves on the array.[21–23]

The present study proposes a sound-field reconstruction method based on an equivalent source model. It makes use of a combination of point sources to describe the sound field on the array. The methodology is analogous to the well-known method of wave superposition or equivalent source method (also known as source simulation method, multipole method)[27–29] with the particularity that the problem is formulated using a Neumann Green's function that accounts for the presence of the rigid sphere array in the medium. Based on this wave expansion, it is possible to reconstruct either the total sound field, or just the incident one (if the free-field Green's function is used for the reconstruction). In this way the scattering introduced by the presence of the rigid sphere is compensated for, making the array virtually transparent. The proposed method is not restricted to reconstruction over spherical surfaces (unlike reconstruction methods based on extrapolating a spherical harmonic expansion), but makes it possible to reconstruct the entire sound field at any point of the source-free domain. Additionally, it makes it possible to use sequential measurements: several measurement positions can be combined, forming an extended measurement area consisting of several spheres. The method will be referred here as "Spherical equivalent source method," S-ESM for brevity.

The existing methods and the theoretical background are presented in Sec. II, leading to the formulation of the method in Sec. III. Numerical and experimental results are presented in Secs. IV and V.

II. THEORETICAL BACKGROUND

A. Existing methods

Throughout this paper, the chosen sign convention is $e^{j\omega t}$ (although the explicit time dependency is omitted), thus

[a)]Portions of this work were presented in "Reconstruction of sound fields with a spherical microphone array," in *Proceedings of Inter-Noise 2014*, Melbourne, Australia, November 2014.
[b)]Electronic mail: efg@elektro.dtu.dk

 0001-4966/2016/139(3)/1168/11/$30.00

spherical Hankel functions of the second kind are used, defined as $h_n^{(2)}(x) = j_n(x) - \mathrm{j}y_n(x)$, where j_n and y_n are the spherical Bessel functions of the first and second kind of order n (the latter also known as Neumann functions).[30] Their derivatives are represented by j_n' and y_n'. A spherical coordinate system is considered $\mathbf{r} = (r, \theta, \phi)$ defined as in Fig. 1. For notational simplicity, we express the angular dependency as $\Omega k \equiv (\theta, \phi)$, and $d\Omega \equiv \sin\theta d\theta d\phi$, so that the integration over the sphere is $\int_\Omega (\cdot) d\Omega \equiv \int_0^{2\pi}\int_0^{\pi}(\cdot)\sin\theta d\theta d\phi$. The spherical harmonics $Y_n^m(\Omega)$ are[30]

$$Y_n^m(\Omega) \equiv Y_n^m(\theta,\phi) \equiv \sqrt{\frac{(2n+1)}{4\pi}\frac{(n-m)!}{(n+m)!}}P_n^m(\cos(\theta))\mathrm{e}^{\mathrm{j}m\phi}, \quad (1)$$

where P_n^m are the associated Legendre functions of degree n and order m. Complex conjugation is denoted by $(\cdot)^*$. Vectors are denoted by a small bold font and matrices by a capital bold font.

The existing reconstruction methods based on measurements with spherical arrays rely on expanding the measured sound field into spherical harmonics, and then make use of the radial functions to reconstruct the sound field elsewhere in free-space.[20–24] The measurement can be performed with an *open sphere* array[24] or with a *rigid sphere* array.[20–22] In the open sphere case, the array is assumed to be transparent, and the incident sound field is expanded using Bessel functions of the first kind as radial functions.[24] When the microphone array is flush-mounted on a rigid sphere, the case considered in this paper, the total sound field measured on the sphere is naturally composed by the incident and the scattered waves, which can be modelled analytically. Expanded into spherical harmonics, the total sound pressure is

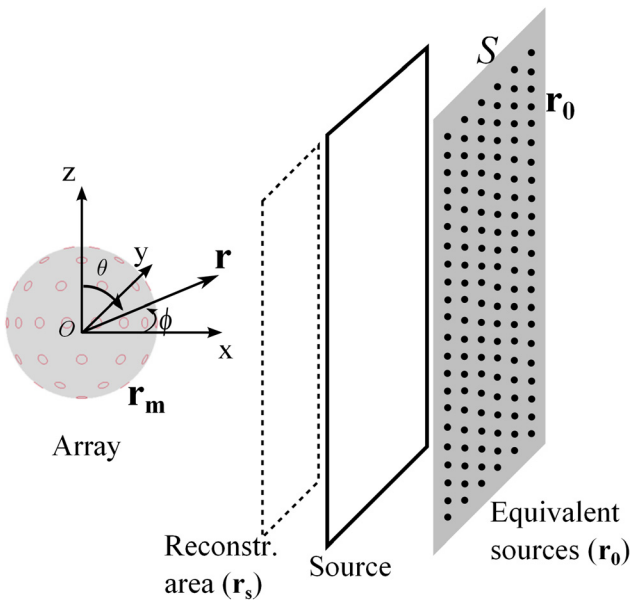

FIG. 1. (Color online) Diagram of a radiation problem using S-ESM. The radiation from an actual acoustic source (a rectangular plate in this diagram) is replaced by the sound field radiated by a set of point sources. The measurement positions are $\mathbf{r_m}$, S the equivalent source surface, $\mathbf{r}_0$ is the equivalent source positions for the discrete case, and $\mathbf{r}$ is the domain, where the reconstruction takes place.

$$p_t(r,\Omega) = \sum_{n=0}^{\infty}\sum_{m=-n}^{n}\mathrm{j}(ka)^2[j_n(kr)h_n'(ka) - j_n'(ka)h_n(kr)] \times Y_n^m(\Omega)\int_\Omega p_t(a,\Omega)Y_n^m(\Omega)^* d\Omega, \quad (2)$$

where a is the radius of the sphere and k is the wavenumber. The term $[j_n(kr)h_n'(ka) - j_n'(ka)h_n(kr)]$ acts as a propagator function, making it possible to extrapolate the sound field from the measurement radius a to a different one r, and thus reconstruct the *total* sound field (incident plus scattered).[20]

It is possible to compensate for the scattering introduced by the rigid sphere by reconstructing the sound field with only the basis functions for the incident field (see Appendix A). This method was originally presented in Ref. 21. The incident pressure can be reconstructed as

$$p_i(r,\Omega) = (ka)^2\mathrm{j}\sum_{n=0}^{\infty}\sum_{m=-n}^{n}h_n'(ka)j_n(kr)Y_n^m(\Omega) \times \int_\Omega p_t(a,\Omega)Y_n^m(\Omega)^* d\Omega. \quad (3)$$

It is easy to see that this incident field p_i is spanned by Bessel functions of the first kind $j_n(kr)$ and the scattered field by Hankel functions $h_n(kr)$ (see Appendix A). This agrees with the expression of the total sound field in Eq. (2).

When reconstructing the incident sound field, the valid domain includes the volumes outside and inside the sphere. When $r \le a$ it is a forward problem, but an inverse problem when $r > a$ (i.e., outside the sphere).[21,22] Finally, it should be noted that Eq. (3) is equivalent to the one given by Jacobsen *et al.* in Ref. 21, although simplified making use of the Wronskian relationship $j_n(ka)h_n'(ka) - j_n'(ka)h_n(ka) = -\mathrm{j}/(ka)^2$.

It is apparent from these equations that the reconstruction of the sound field based on these methods relies on extrapolating the radial functions $j_n(kr)$ and $h_n(kr)$ from the measurement radius a to another arbitrary radius r. This expansion, being a solution to the Helmholtz equation, is valid for the source-free medium, i.e., between the radius of the sphere $r = a$ (or inside $r < a$) and the minimum distance from the center of coordinates to a source $r = r'$. In other words, the reconstruction can take place in spherical surfaces concentric to the arrays that are contained in the source-free region. This imposes a limit in the reconstruction very close to a source, unless the source is approximately conformal to the array surface, an atypical general scenario. Other issues associated to these methodologies are that the spherical harmonic expansion used to extrapolate the sound field needs to be truncated due to the spatial sampling on the sphere,[22,26] and that the problem is ill-conditioned when the reconstruction takes place outside the sphere $r > a$, especially at low frequencies.[20,22,26]

B. Sound field due to a point source

We consider a point source at $\mathbf{r}_0 = (r_0, \theta_0, \phi_0)$ with volume velocity Q, radiating in the presence of a rigid sphere centered in the origin of coordinates. The incident sound pressure, without the scattering introduced by the sphere is

$$p_i = \frac{\mathrm{j}\omega\rho Q \mathrm{e}^{-\mathrm{j}kR}}{4\pi R}, \tag{4}$$

where $R = |\mathbf{r}_0 - \mathbf{r}|$ is the distance between the observation point and the position of the point source. The free-field Green's function is

$$G(\mathbf{r}, \mathbf{r}_0) = \frac{\mathrm{e}^{-\mathrm{j}kR}}{4\pi R}. \tag{5}$$

The resulting total pressure on the sphere's surface (a, Ω_m), i.e., incident plus scattered fields, is well known (originally addressed in Ref. 31). Here the solution in Ref. 32 expressed as in Ref. 20 is used, and simplified via the Wronskian, because we consider the field on the boundary $r = a$ (see Ref. 26),

$$p_t(a, \Omega_m) = \frac{-\mathrm{j}\rho c Q}{a^2} \sum_{n=0}^{\infty} \sum_{m=-n}^{n} \frac{h_n(kr_0)}{h_n'(ka)} Y_n^m(\Omega_m) Y_n^m(\Omega_0)^*, \tag{6}$$

where (r_0, Ω_0) is the position of the point source (because of the rotational axisymmetry, it is often expressed with Legendre polynomials).

It is interesting to note that the expansion of a plane wave into spherical harmonics is similar to Eq. (6) but without the Hankel function $h_n(kr_0)$ that accounts for the spherical spreading[6,14,30]

$$p_t(a, \Omega_m) = \frac{4\pi A}{(ka)^2} \sum_{n=0}^{\infty} \sum_{m=-n}^{n} \frac{(-\mathrm{j})^{n+1}}{h_n'(ka)} Y_n^m(\Omega_m) Y_n^m(\Omega_0)^*. \tag{7}$$

This expression would serve to formulate a plane wave expansion, which is a useful reconstruction basis for cases where the decay of the waves in the sound field can be neglected.[14]

Equation (6) can be expressed via a Neumann Green's function, $p_t = \mathrm{j}\omega\rho Q G_N(\mathbf{r}, \mathbf{r}_0)$, with $G_N = G + g_N$ (see Ref. 30 [Eq. 8.85]), where G is the homogeneous solution due to the incident field, i.e., Eq. (4), and g_N is the non-homogeneous solution due to the scattering by the rigid sphere. On the surface of the sphere, the resulting Neumann Green's function is

$$G_N\left(\mathbf{r}|_{r=a}, \mathbf{r}_0\right) = -\frac{1}{ka^2} \sum_{n=0}^{\infty} \sum_{m=-n}^{n} \frac{h_n(kr_0)}{h_n'(ka)} Y_n^m(\Omega) Y_n^m(\Omega_0)^*, \tag{8}$$

in direct agreement with Eq. (6).

III. METHOD

A. Point source expansion

The S-ESM method proposed in this paper consists of expressing an arbitrary sound field on a rigid sphere as the superposition of waves radiated by a combination of monopoles, i.e., using as a basis the sound field due to multiple point sources. This is fundamentally an extension of the equivalent source method[28,29] to measurements with a rigid spherical microphone array.

The sound pressure measured on each of the M transducers of the rigid spherical array can be expressed as a continuum of point sources over the surface S associated with $\mathbf{r}_0 = (r_0, \Omega_0)$, i.e., the surface over which the point sources are distributed; see Fig. 1,

$$p_t(a, \Omega_m) = \int_S \frac{-\mathrm{j}\rho c U(\mathbf{r}_0)}{a^2} \times \sum_{n=0}^{\infty} \sum_{m=-n}^{n} \frac{h_n(kr_0)}{h_n'(ka)} Y_n^m(\Omega_m) Y_n^m(\Omega_0)^* dS, \tag{9}$$

where U is the surface velocity $[\mathrm{m\,s^{-1}}]$ on S.

In practice, the surface S can be placed inside the actual source under study (retracted from the surface of the source, as in Fig. 1), outside the domain in which the sound field is reconstructed, to prevent the singularities. If no *a priori* knowledge on the source is assumed, the equivalent sources can be distributed all around the array, as shown in Fig. 2, to model the wave field in the volume about the array. If the distribution of sources from Eq. (9) is discretized

$$p_t(a, \Omega_m) = \sum_{l=1}^{L} \frac{-\mathrm{j}\rho c Q_l}{a^2} \times \sum_{n=0}^{\infty} \sum_{m=-n}^{n} \frac{h_n(kr_{0,l})}{h_n'(ka)} Y_n^m(\Omega_m) Y_n^m(\Omega_{0,l})^*, \tag{10}$$

where Q_l is the volume velocity of each equivalent source. Conducting the summation over n and m, truncated at $n = N$, it is possible to express the total sound pressure $\mathbf{p}_t \in \mathbb{C}^M$ at a discrete set of M points on the sphere as

$$\mathbf{p}_t = \mathbf{G}_N \mathbf{q}, \tag{11}$$

where the vector $\mathbf{q} \in \mathbb{C}^L$ consists of the unknown complex coefficients that we want to solve for, often referred to as "source strengths," and which correspond to the mass

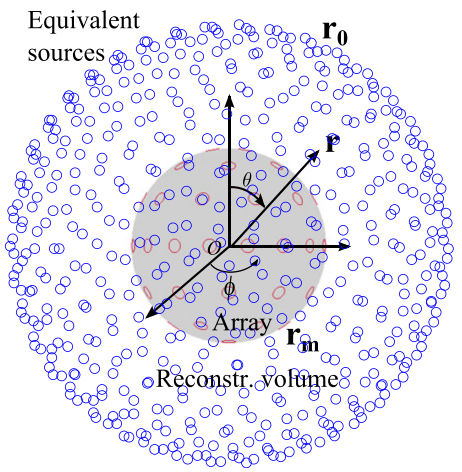

FIG. 2. (Color online) Illustration of an equivalent source distribution used to model the wave field around the array.

acceleration $j\omega\rho Q_l$ in Eq. (10); ωQ_l is the volume acceleration. The matrix $\mathbf{G}_N \in \mathbb{C}^{M\times L}$ contains the Neumann Green's function [Eq. (8)], between measurement positions and equivalent sources. This is an ill-conditioned problem, typically underdetermined $(M < L)$, that ought to be inverted using regularization. This is addressed in Sec. III B.

Once the strength of the sources has been determined, the incident component of the sound pressure $\mathbf{p}_i \in \mathbb{C}^K$ can be predicted anywhere in the domain

$$\mathbf{p}_i = \mathbf{G}\,\mathbf{q}, \tag{12}$$

where the reconstruction matrix $\mathbf{G} \in \mathbb{C}^{K\times L}$ corresponds to the *free-field* Green's function, i.e., Eq. (5), between the equivalent sources in $\mathbf{r}_0$ and the reconstruction points $\mathbf{r}_s$. This evidences the fact that the scattering introduced by the sphere is compensated for. The reconstruction could alternatively be based on the Neumann Green's function, as in Eq. (11), to obtain the total sound field.

The particle velocity vector can be calculated from Euler's equation of motion, $\mathbf{u} = -\nabla p/(j\omega\rho)$, thus

$$\mathbf{u}_i = \frac{-1}{j\omega\rho}\nabla\mathbf{G}\,\mathbf{q}, \tag{13}$$

where $\nabla\mathbf{G}$ is a matrix with the gradient of the Green's function with respect to the normal of S. Correspondingly the sound intensity vector at each reconstruction point is obtained as

$$\mathbf{I}_i = \frac{1}{2}\mathrm{Re}\{p\,\mathbf{u}^*\}, \tag{14}$$

where the superscript $*$ denotes the complex conjugate. The full sound intensity vector can be calculated via the Hadamard product of the reconstructed sound pressure vector and the complex conjugate of the particle velocity, i.e., Eqs. (12) and (13). It is apparent from these equations that the reconstruction provides a complete characterization of the incident acoustic field—sound pressure, velocity, intensity, and power.

In summary, the proposed S-ESM method can be used for reconstructions over arbitrary geometries and the scattering introduced by the array can be compensated for. The formulation allows for combined sequential measurements calculating a transfer matrix as in Eq. (11) but translating the array to the different measurement positions, to estimate the source strengths from the combined measurements. This leads to having an array of spheres as a measurement system.

Finally, it is remarked that the representation of the acoustic field over the reconstruction space is based on the wave superposition method, which is well known to be a good model for sound radiation and scattering problems of arbitrary sources.[27–29] A brief comparison with the S-NAH method is included in Sec. IV B.

B. Regularized solution to the problem

The solution of Eq. (11) can be calculated in a least-squares sense, i.e., via a regularized matrix pseudo-inverse. It follows that the solution of the expansion coefficients does not rely on explicit numerical integration on the sphere. The problem formulated in Eq. (11) can be cast in a general sense as an optimization problem of the form

$$\min_{\mathbf{q}} \|\mathbf{q}\|_p^p \quad \text{subject to } \mathbf{p}_t = \mathbf{G}_N\mathbf{q}, \tag{15}$$

where the choice of the p-norm will result in different penalties to the problem, and therefore condition the solution that is sought. In the presence of noise, the problem can also be formulated as

$$\min_{\mathbf{q}} \|\mathbf{q}\|_p^p \quad \text{subject to } \|\mathbf{G}_N\mathbf{q} - \mathbf{p}_t\|_2 \le \epsilon, \tag{16}$$

where ϵ is the upper bound of the noise vector. Alternatively, the problem can be formulated as an unconstrained problem, introducing a regularization parameter μ, that will determine the penalty weight of the p-norm of the solution vector

$$\min_{\mathbf{q}} \|\mathbf{G}_N\mathbf{q} - \mathbf{p}_t\|_2^2 + \mu\|\mathbf{q}\|_p^p. \tag{17}$$

Throughout this work the 2-norm of the solution is chosen

$$\min_{\mathbf{q}} \|\mathbf{G}_N\mathbf{q} - \mathbf{p}_t\|_2^2 + \mu\|\mathbf{q}\|_2^2, \tag{18}$$

which conveniently has the well-known closed form analytical solution

$$\mathbf{q} = \mathbf{G}_N^H(\mathbf{G}_N\mathbf{G}_N^H + \mu\mathbf{I})^{-1}\mathbf{p}_t, \tag{19}$$

where the superscript H denotes the conjugate transpose and $\mathbf{I}$ is the identity matrix. Equation (19) corresponds to the least squares solution of the problem with Tikhonov regularization.[22,33] The right inverse is chosen because it is more efficient computationally for an underdetermined problem like the one addressed here $(L > M)$, given the dimensions of the product $\mathbf{G}_N\mathbf{G}_N^H$ compared to $\mathbf{G}_N^H\mathbf{G}_N$ of the left inverse. The obtained solution makes it possible to use Eqs. (12)–(14) to reconstruct the sound field.

Although the ℓ_2-norm solution is chosen in this work, there are alternative solutions, such as the ℓ_1-norm,[14] that promote sparse solutions, i.e., few non-zero coefficients, implicitly acting as a regularization penalty. For sparse signals, the solution from the ℓ_1 is equivalent to the ℓ_0 (pseudonorm) minimization, but forming a convex optimization problem that can be solved efficiently via quadratic programming.[14,34] This approach is presented in a separate study, see Ref. 14.

IV. NUMERICAL RESULTS

A. S-ESM

A simulation is conducted to examine the accuracy of the proposed method (S-ESM) and some of its numerical properties. The array used for the simulated measurements is a 9.75 cm radius rigid-sphere array with 50 microphones, with near-uniform sampling (see the Appendix in Ref. 21), which can sample up to $N = 5$ orders of spherical harmonics. The array is centered in the origin of coordinates, and the source

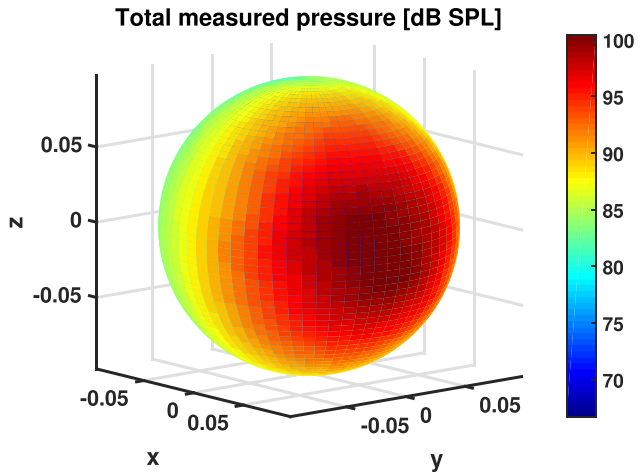

FIG. 3. (Color online) Measured pressure on the spherical array with $M = 50$ microphones (interpolated for clarity).

consists of a pair of monopoles in quadrature, with volume velocities $Q_1 = 10^{-4}$ m^{3}s^{-1} and $Q_2 = \mathrm{j}10^{-4}$ m^{3}s^{-1}, separated 8 cm from each other, aligned in a plane that is 15 cm away from the origin of coordinates (thus 5.25 cm away from the array's surface). The equivalent sources used to model the sound field are distributed over a 21×21 planar mesh, covering a 10×10 cm^2 surface, and retracted 1 cm behind the actual source plane (note that the aim is to model the radiation of the actual source using a set of point sources. Therefore these are slightly retracted to avoid their singularity—as in Fig. 1). Normally distributed noise of 30 dB signal-to-noise ratio is added to the simulated measurements. For the regularized inversion of the problem, Tikhonov regularization is used and the regularization parameter selected with generalized-cross-validation.[22,33] The reconstruction takes place over a plane of dimensions 10×10 cm^2 conformal to the equivalent sources, close to the array, at $x = 10$ cm distance from the array center and 5 cm away from the source (the center of the reconstruction area is 0.25 cm and the corner 2.5 cm away from the array's surface).

Figure 3 shows the sound pressure level on the surface of the spherical array at a frequency of 1000 Hz (Helmholtz nr. $ka \approx 1.8$). Figure 4 shows the reconstructed sound field over a 10×10 cm^2 plane at $x = 10$ cm, and compared to the "true" reference sound field, which is calculated based on the analytical field radiated by the monopoles. Figure 4 (left) shows the reconstruction of the sound pressure, which is fairly accurate. Figure 4 (center) shows the normal component of the particle velocity, where a greater reconstruction error is apparent, particularly toward the edges of the reconstruction aperture, due to the larger back-propagation distance and therefore greater ill-conditioning of the problem there. In general, the reconstruction of the particle velocity from pressure measurements is considerably more ill-posed than the reconstruction of the pressure field, because the particle velocity is proportional to the gradient of the sound pressure, thus promotes rapid spatial changes of the sound field, which are often due to measurement noise rather than the actual sound field. Finally, Fig. 4 (right) shows the reconstructed normal component of the active intensity vector. There also exist noticeable deviations, especially toward the edges of the aperture, in accordance to the observed results of the sound pressure and particle velocity.

Figure 5 shows the normalized error point by point over the reconstruction plane (without spatial averaging, calculated as a Hadamard $\oslash$ pointwise division),

$$\mathbf{E}[\mathrm{dB}] = 20\log(|\mathbf{x} - \tilde{\mathbf{x}}| \oslash |\mathbf{x}|), \tag{20}$$

where the vector $\mathbf{x}$ corresponds to the true quantity (pressure, particle velocity, or sound intensity) and $\tilde{\mathbf{x}}$ to the reconstructed

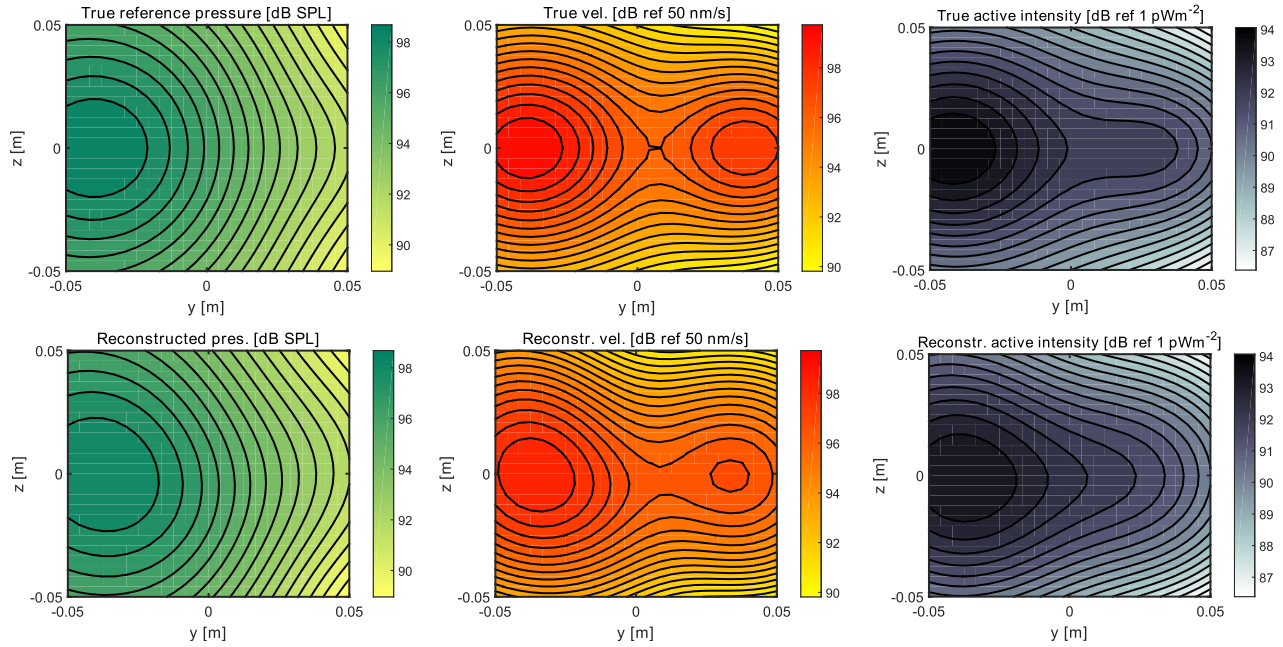

FIG. 4. (Color online) True and reconstructed sound field over a planar surface in front of the array. Left: true (top) and reconstructed (bottom) sound pressure; center: true (top) and reconstructed (bottom) particle velocity; right: center: True (top) and reconstructed (bottom) sound intensity. Frequency 1 kHz.

quantity. Also the spatially averaged relative error (in percent), is given

$$\langle \epsilon \rangle [\%] = \frac{\|\mathbf{x} - \tilde{\mathbf{x}}\|_2}{\|\mathbf{x}\|_2} 100, \tag{21}$$

where $\|\cdot\|_2$ indicates the ℓ_2-norm of the vectors.

The error plots in Fig. 5 corroborate that the reconstruction of the sound pressure is more accurate than that of the particle velocity and active intensity. The reconstruction error is greater toward the edges of the aperture as discussed earlier. It should be noted that the error depends considerably on the choice of regularization parameter (which can be chosen manually, or automatically based on well-known parameter-choice methods).[33] If a too low parameter is chosen, the reconstruction is under-regularized and most likely meaningless. Conversely, if a somewhat large regularization parameter is chosen the solution is over-regularized. If the over-regularization is not too drastic the reconstruction can be acceptable, although a bias-like error results, in which the profile of the reconstruction is approximately correct but the recovered power is slightly under-estimated, due to discarding some energy of the solution that in reality corresponds to the actual signal [this also follows from the energy minimization constrain imposed in the 2-norm solution as in Eq. (18)].

Figure 6 shows a box plot of the spatially averaged error as a function of frequency for the same source used before. The errors have been computed for 25 separate realizations, over a frequency range from 50 to 3000 Hz. The reconstruction is over a $10 \times 10\,\mathrm{cm}^2$ aperture and the reconstruction plane is again 10 cm from the center of the array. In this case the equivalent sources were retracted 2 cm behind the source ($x = 17$ cm). The circled dots in the figure are the median of the error, the box represents the first and third quartiles (error between the 25% and 75% percentile), and the whiskers (thin lines) are 1.5 times the interquartile distance (as in a Tukey box plot). Outliers outside this range have been removed since they represent meaningless reconstructions due to wrong automatic-choice regularization parameters that would anyway be detectable. The results show that the method is robust. The slightly greater error in the velocity and intensity reconstructions is due to the greater ill-conditioning for the back propagated reconstruction (for the forward problem all errors fall below 10%—Fig. 7).

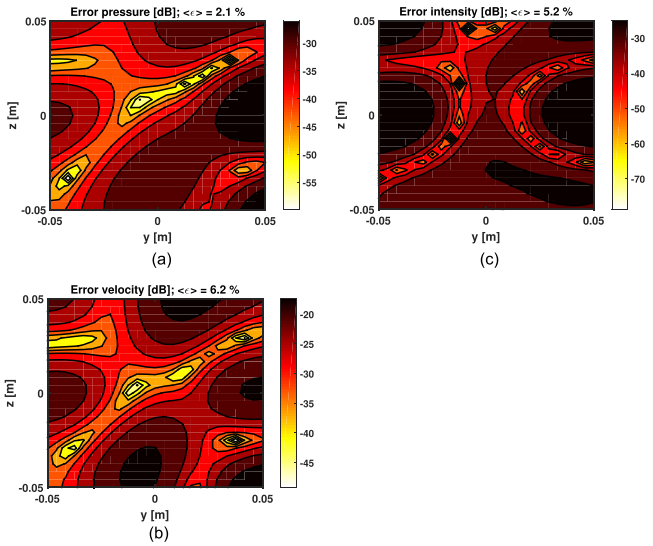

FIG. 5. (Color online) Relative error of pressure, particle velocity, and sound intensity $20\log(|\mathbf{x} - \tilde{\mathbf{x}}| \oslash |\mathbf{x}|)$ where $\mathbf{x}$ is the true field and $\tilde{\mathbf{x}}$ is the reconstructed field. Also the spatially averaged error is given in %.

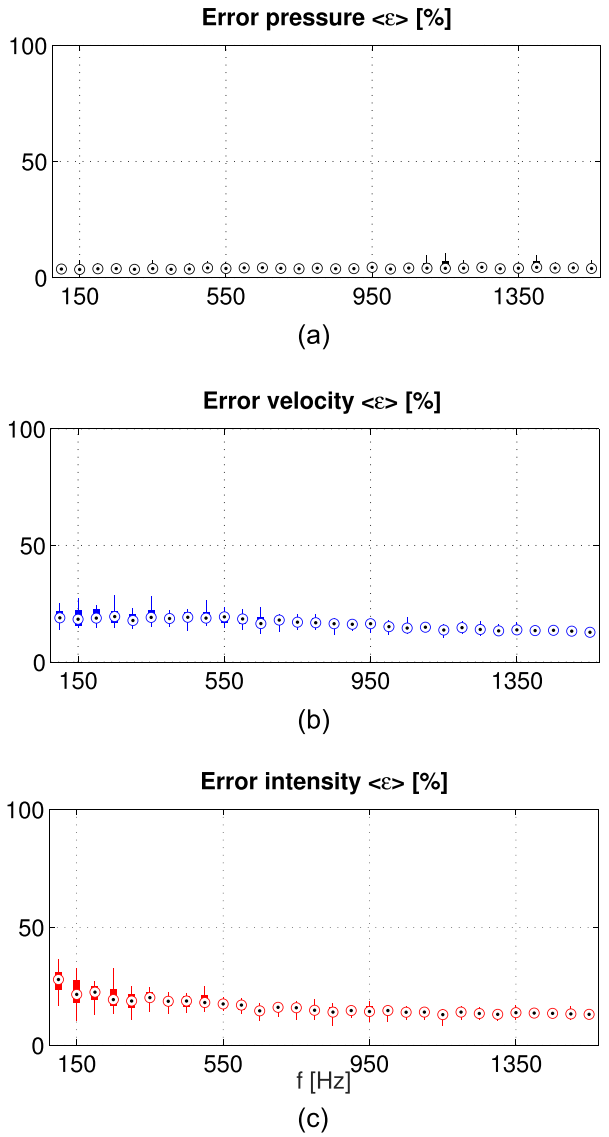

FIG. 6. (Color online) Relative error of pressure, particle velocity, and sound intensity $20\log(\|\mathbf{x} - \tilde{\mathbf{x}}\|_2 / \|\mathbf{x}\|_2)$ where $\mathbf{x}$ is the true field and $\tilde{\mathbf{x}}$ the reconstructed/estimated field.

Figure 7 shows the reconstruction error as a function of the reconstruction position at $f = 1000$ Hz; when the reconstruction plane is moved along the x coordinate—the axis between the center of the array and the source (see coordinates in Fig. 3 for guidance). The accuracy of the reconstruction is good whenever $x_s < 0$ (meaning that the reconstruction takes place further away from the array) because in this case it is a forward problem. Contrarily, when the reconstruction takes place in the space between the array and the source, the reconstruction error increases notably because of the greater ill-conditioning of the problem due to the back-propagation. It follows from these

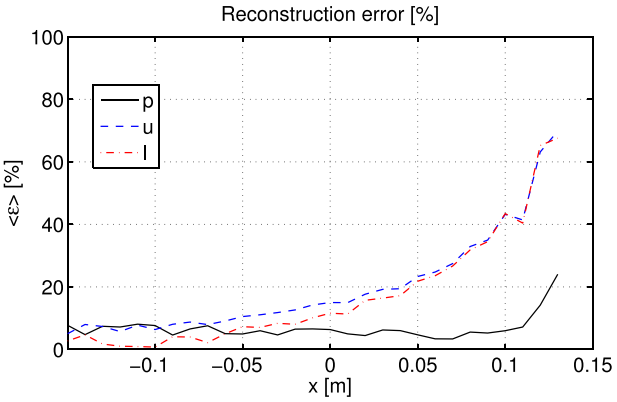

FIG. 7. (Color online) Spatially averaged reconstruction error as a function of position: normalized error over the reconstruction plane for different reconstruction distances from $x = -20$ cm (forward propagation) to $x = 0.13$ (back-propagation, just in front of the source).

results, and in agreement with the previous observation, that the estimation of particle velocity and sound intensity is accurate as long as the reconstruction does not take place closer to the source than measured, see Appendix B. The greater error could nevertheless be alleviated via suitable pre-conditioning.

B. Comparison with spherical harmonic extrapolation

In this section, the proposed method is compared to spherical near-field acoustic holography (SNAH),[21] which is based on an extrapolation of the radial functions in the spherical harmonic expansion as described by Eq. (3).[26] A more extensive comparison will be the subject of a future publication.

The source used for this test is a monopole, placed 40 cm away from the center of the array, with volume velocity of 10^{-5} m^3/s. An equivalent source grid of 20×20 sources over a 10×10 cm^2 plane, 41 cm away from the center of the array. Additive noise of 30 dB signal-to-noise ratio relative to the measured pressure is included in the simulated measurements. For both methods, the regularization used is truncated singular value decomposition.[22] The reconstruction is on the line passing through the monopole and the center of the array, as shown in Fig. 8.

Figure 9 shows the results from the reconstruction. The proposed method (S-ESM) is notably more accurate, especially in the region far from the array and sound source, where it is a forward problem, unlike the SNAH method. In

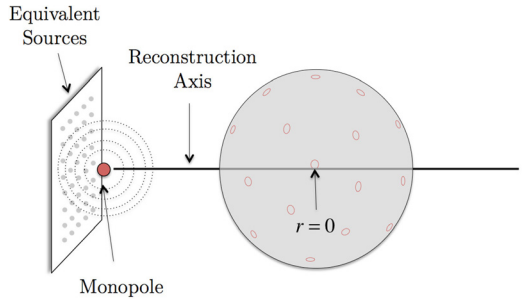

FIG. 8. (Color online) Diagram showing the set up for SNAH and S-ESM comparison.

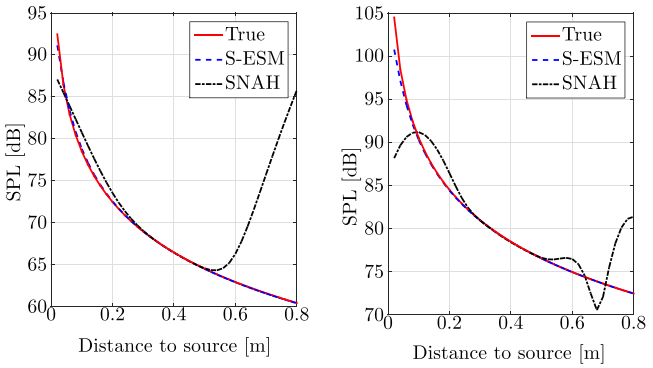

FIG. 9. (Color online) Comparison of methods: true pressure (solid line); proposed S-ESM method (dashed line); SNAH method (dashed-dotted line). Left: $ka = 0.5$. Right: $ka = 2$.

fact, the numerical properties of the S-ESM method constitute a fundamental difference with respect to the spherical harmonic expansion methods (see Sec. II A): the S-ESM reconstruction is an inverse problem when the reconstruction takes place between the array and the equivalent sources, but otherwise it is a forward problem. Contrarily, in the SNAH reconstruction [Eq. (3)], the problem is inverse whenever $r > a$ in all angular directions (i.e., anywhere outside the sphere), regardless of whether the reconstruction takes place closer or further to the acoustic source.[20,21] This is due to the basis used, i.e., the amplification introduced by the radial functions for $r > a$.

In the general case, the equivalent source method is more suitable for modeling radiation problems, and more appropriate than a spherical harmonic expansion truncated at $N = 5$ for representing an arbitrary sound field about the array. Additionally, conventional regularization strategies for the inversion can be used.[26]

A more extensive comparison between the S-ESM method and the existing spherical harmonic expansions is out of the scope of this paper. This will be published in a separate study.

V. EXPERIMENTAL RESULTS

An experiment on a vibrating plate was conducted to examine the proposed method. In this experiment, we combine multiple measurement positions acquired sequentially, in order to obtain a larger measurement area that spans the dimensions of the actual source. The source considered is a 40×60 cm^2 aluminum plate 1.5 mm thick mounted on a metal box, as shown in Fig. 10. The box was placed in the DTU anechoic chamber, hanging from the ceiling and driven at the bottom with a shaker. The array used is a mixed ambisonics array[17,18] of radius 5 cm, with 52 microphones, non-uniformly spaced, which provide a finer azimuth than elevation resolution and can sample up to 5 spherical harmonics. The spherical harmonic expansion was nonetheless truncated at $N = 4$.

Six positions were measured sequentially as depicted in Fig. 10 (right), virtually forming an array of six spheres, which covered about 20% of the total area of the plate. The array was placed 5 cm away from the plate. The equivalent

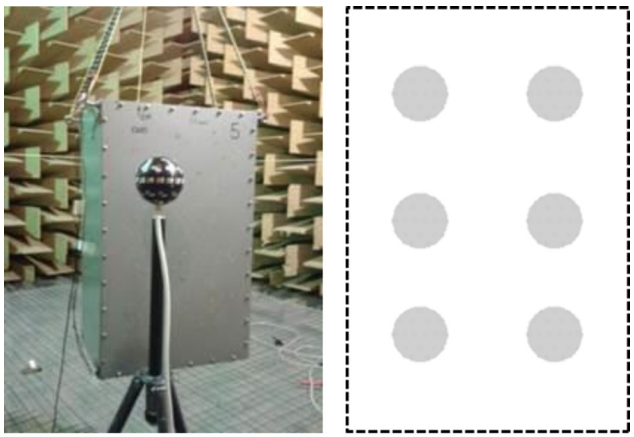

FIG. 10. (Color online) Setup of the experiment (left); six sequential measurement positions (right).

source grid used is 40×60 sources, retracted 2 cm from the surface of the plate. In this case, the problem is formulated by constructing a row-wise augmented matrix system, that contains the $T = 6 \times M$ measurement points

$$\mathbf{P} = \mathbf{H}\,\mathbf{q}, \tag{22}$$

where the strength of the equivalent sources $\mathbf{q} \in \mathbb{C}^L$ model the radiation of the source as usual, distributed conformally to it, and $\mathbf{P}$ is an augmented vector containing all measurement positions ($6 \times M = 312$ in this specific measurement)

$$\mathbf{P} = [\mathbf{p}_1, \mathbf{p}_2, \ldots, \mathbf{p}_6],$$

$$\mathbf{H} = [\mathbf{G}_1, \mathbf{G}_2, \ldots, \mathbf{G}_6],$$

where $\mathbf{P} \in \mathbb{C}^T$ and $\mathbf{H} \in \mathbb{C}^{T \times L}$, $T = 6M$ being the total number of microphone positions. Note that each of the submatrices $\mathbf{G}_n$ is a translated version of Eq. (8), i.e., the relative positions between the array and equivalent sources are shifted.

The vibrating plate is an interesting source because it is larger than the array, and far from spherical, hence a good test for the proposed method. The plate was driven with white noise, and 2 s Hanning windows are used for the fast Fourier transform analysis. A separate microphone was set as a fixed phase reference to carry out the sequential measurements. We use Tikhonov regularization and the L-curve criterion as a parameter-choice method. The reconstruction plane is 3 cm away from the plate.

Figure 11 shows the reconstructed sound pressure and normal component of the particle velocity at 178 Hz, at a natural frequency corresponding to an operational deflection shape close to a (3,1) mode. Figure 12 shows the frequency of 209 Hz corresponding to a (2,2) mode-like deflection shape. These modes are clearly identified in the results from the reconstruction. Because the plate is not baffled, but mounted on a box, there are also contributions from the other five faces of the box. This explains the increase of the pressure and particle velocity toward the edge of the plate, which is particularly apparent in Fig. 11.

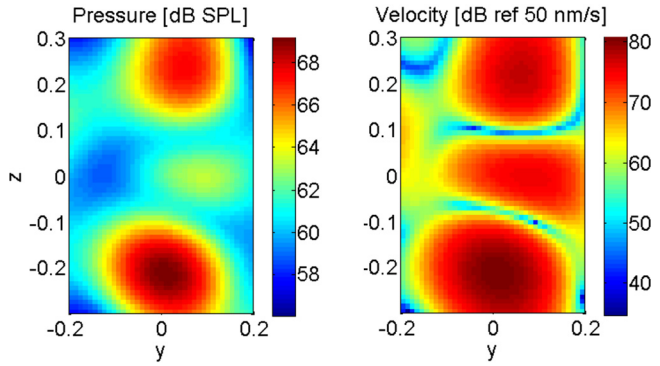

FIG. 11. (Color online) Reconstructed sound pressure and particle velocity at 178 Hz, identifiable deflection shape close to a (3,1) mode.

The quantitative validity of the method across frequency is shown in Fig. 13. The figure shows a reconstruction of the sound pressure and compares it directly to the sound pressure measured with a 1/2 in. B&K (Nærum, Denmark) free-field microphone. For this measurement, a single array measurement position is used (as in Sec. IV), and the array center is placed at $(x, y, z) = (7.5, -5, 0)$ cm. The reconstruction takes place at a point 1 cm in front of the plate, i.e., $(1, -5, 0)$ cm, for frequencies ranging from 100 Hz ($ka \approx 0.1$) to 1 kHz ($ka \approx 1$). The results of the quantitative validation show that the reconstructed and true reference fields agree fairly well for most of the frequency range. Deviations are larger at very low frequencies: below 120 Hz, where the size/circumference of the sphere corresponds to about 10% of the wavelength in air ($ka = 0.1$), as well as at high frequencies. Above 900 Hz spatial aliasing effects start to appear (there are short wavelengths associated with the evanescent waves radiated by the plate below its critical frequency at $f_c \approx 8$ kHz. Because the spherical harmonic expansion is truncated at $N = 4$, the expected aliasing limit $k_b a < N$ is met at approximately 850 Hz, due to the bending waves borne in the plate). In the frequency range of validity, the reconstruction results are accurate, and the overall performance of the method satisfactory. There are larger deviations in the dips corresponding to nodes on the plate, where small positioning errors become significant, due to rapid changes in the sound field.

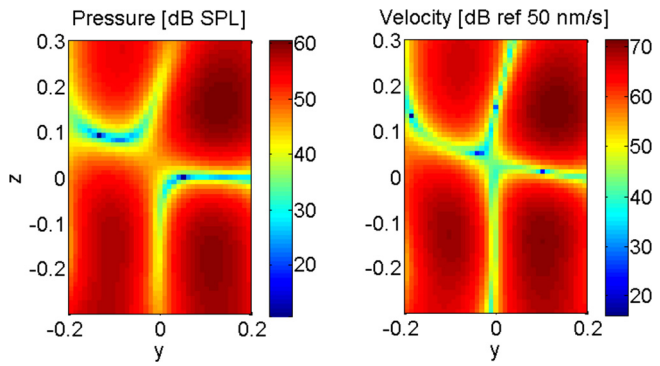

FIG. 12. (Color online) Reconstructed sound pressure and particle velocity at 209 Hz, identifiable deflection shape close to a (2,2) mode.

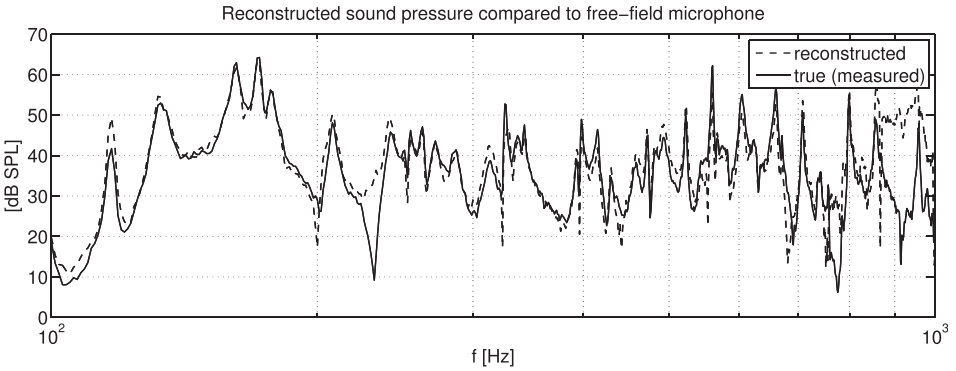

FIG. 13. Sound pressure reconstruction at a point 2 cm in front of the vibrating plate, compared to measurements with a 1/2′ microphone (structural wavelength at 900 Hz is approximately 11 cm).

VI. CONCLUSIONS

A method to reconstruct sound fields using a rigid sphere microphone array is proposed in this study (S-ESM). The method is based on a point source expansion, and can be understood as a version of the method of wave superposition or equivalent source method, in which the presence of the rigid sphere is taken into account via a Neumann Green's function. Naturally it can yield all the acoustic quantities, i.e., sound pressure, particle velocity, and sound intensity in a different surface than measured. Both the total sound field and only the incident field can be obtained, compensating for the scattering introduced by the array.

Due to the basis functions used, and contrary to existing methods, it is possible to reconstruct the sound field over arbitrary geometries and perform sequential measurements (combine several measurements with the array placed at different positions). The equivalent source model can be designed making use of *a priori* information—for instance regarding the position of the sound sources, to improve accuracy and numerical conditioning. Furthermore, because of being formulated as an elementary wave model, the solution can be obtained in a least-squares sense using conventional regularized inversion schemes, but allows for alternative solution strategies (ℓ_1-norm, etc.), conveying an interesting prospect in further work.[14]

The numerical and experimental results show that the method is accurate and robust. Its accuracy depends on the ill-conditioning of the specific reconstruction: In the forward problem, the resulting error for the entire sound field reconstruction (pressure, velocity, and intensity) is below 10%. However, in the inverse problem solution the error increases notably, especially for the particle velocity and intensity. The quantitative validity of the method has been shown experimentally using a vibrating plate as the source under study, and shows good agreement with direct measurements conducted with a calibrated free-field microphone.

ACKNOWLEDGMENTS

The author would like to thank Marton Marschall for his input and help with the measurement setup, Tim Walton for the S-NAH numerical data, and Mélanie Nolan, Angeliki Xenaki, and Antoine Richard for comments and discussion. This work was supported by the Danish Council for Independent Research (DFF), under the individual postdoctoral Grant No. FTP/12-126364.

APPENDIX A: SPHERICAL HARMONIC RECONSTRUCTION

This appendix shows the derivation of the boundary value problem leading to Eqs. (3) and (4), corresponding to the reconstruction of the sound field based on a spherical harmonic expansion.

Let there be a rigid sphere immersed into the sound field, which scatters sound, giving rise to a total sound pressure

$$p_t(r,\Omega) = p_i(r,\Omega) + p_s(r,\Omega), \tag{A1}$$

where p_t is the total pressure, p_i is the incident pressure, and p_s is the scattered sound pressure due to the sphere. In a spherical coordinate system, the total sound pressure is expanded as $p_t(r,\Omega) = \Sigma_{n=0}^{\infty}\Sigma_{m=-n}^{n} A_{mn} h_n(kr) Y_n^m(\Omega)$. The incident field is expanded similarly, although only the spherical Bessel functions of the first kind are used, since the Neumann functions are singular at the origin. For physical plausibility (finiteness at the origin) the incident field must be

$$p_i(r,\Omega) = \sum_{n=0}^{\infty}\sum_{m=-n}^{n} B_{mn} j_n(kr) Y_n^m(\Omega). \tag{A2}$$

The scattered field only exists outside of the sphere, and has a radiation solution of the form

$$p_s(r,\Omega) = \sum_{n=0}^{\infty}\sum_{m=-n}^{n} C_{mn} h_n(kr) Y_n^m(\Omega). \tag{A3}$$

The boundary condition dictates that the radial component of the particle velocity must vanish on the rigid sphere, since no fluid motion is possible, i.e., $(\partial p_t(r,\Omega)/\partial r)|_{r=a} = 0$. This combined with Eqs. (A2) and (A3),

$$B_{mn} j_n'(ka) + C_{mn} h_n'(ka) = 0. \tag{A4}$$

The total sound field, from Eqs. (A2) and (A3), making use of (A4), results in

$$p_t(r,\Omega) = \sum_{n=0}^{\infty}\sum_{m=-n}^{n} B_{mn}\left(j_n(kr) - \frac{j_n'(ka)}{h_n'(ka)} h_n(kr)\right) Y_n^m(\Omega). \tag{A5}$$

Because the pressure p_t is measured, it is possible to calculate the coefficients of the expansion from Eq. (A5),

$$B_{mn} = \frac{\int_\Omega p_t(a,\,\Omega) Y_n^m(\Omega)^* d\Omega}{j_n(ka) - \frac{j_n'(ka)}{h_n'(ka)} h_n(ka)}, \tag{A6}$$

where the orthogonality of the spherical harmonics has been used, $\int Y_n^m(\Omega) Y_{n'}^{m'}(\Omega)^* d\Omega = \delta_{nm}\delta_{n'm'}$. The integral $\int_\Omega p_t(a,\Omega) Y_n^m(\Omega)^* d\Omega$ corresponds to the so-called spherical Fourier coefficients P_{nm} that result from the Fourier series $p_t(a,\Omega) = \Sigma_{n=0}^{\infty} \Sigma_{m=-n}^{n} P_{nm} Y_n^m(\Omega)$. Making use of the Wronskian relationship, the coefficients B_{mn} can be expressed as

$$B_{mn} = \mathrm{j}(ka)^2 h_n'(ka) \int_\Omega p_t(a,\,\Omega) Y_n^m(\Omega)^* d\Omega, \tag{A7}$$

and the coefficients for the scattered field from Eq. (A4),

$$C_{mn} = \mathrm{j}(ka)^2 j_n'(ka) \int_\Omega p_t(a,\,\Omega) Y_n^m(\Omega)^* d\Omega. \tag{A8}$$

The total sound field, from Eqs. (A2) and (A3) and inserting B_{mn} and C_{mn}, can be expressed as

$$p_t(r,\Omega) = \mathrm{j}(ka)^2 \sum_{n=0}^{\infty} \sum_{m=-n}^{n} \left(j_n(kr) h_n'(ka) - h_n(kr) j_n'(ka)\right) \times Y_n^m(\Omega) \int_\Omega p_t(a,\,\Omega) Y_n^m(\Omega)^* d\Omega, \tag{A9}$$

as shown in Eq. (2). Remarkably, via Eqs. (A2) and (A8), it is possible to reconstruct the incident sound field separately, i.e., the sound field without the scattering introduced by the sphere, as if the array was not present. The resulting expression is the one given in Eq. (3), Sec. II A,

$$p_i(r,\,\Omega) = (ka)^2 \mathrm{j} \sum_{n=0}^{\infty} \sum_{m=-n}^{n} h_n'(ka) j_n(kr) Y_n^m(\Omega) \times \int_\Omega p_t(a,\,\Omega) Y_n^m(\Omega)^* d\Omega.$$

APPENDIX B: NUMERICAL CONDITIONING

The condition number of a matrix indicates the sensitivity of the system's solution to small perturbations in the observed data. An upper bound of the ill-conditioning with respect to reconstruction position is shown in Fig. 14, where the full reconstruction process is considered: combining Eqs. (11) and (12) results in $\mathbf{p}_i = \mathbf{G}\mathbf{G}_N^+ \mathbf{p}_t$ or equivalently $\mathbf{p}_t = \mathbf{G}_N \mathbf{G}^+ \mathbf{p}_i$; the latter can be seen as a transfer matrix between the sought solution and the measured data, which should be inverted to obtain $\mathbf{p}_i$. For invertible matrices, an upper bound of the condition number is given by

$$\kappa(\mathbf{G}_N \mathbf{G}^+) \leq \kappa(\mathbf{G}_N)\kappa(\mathbf{G}^+), \tag{B1}$$

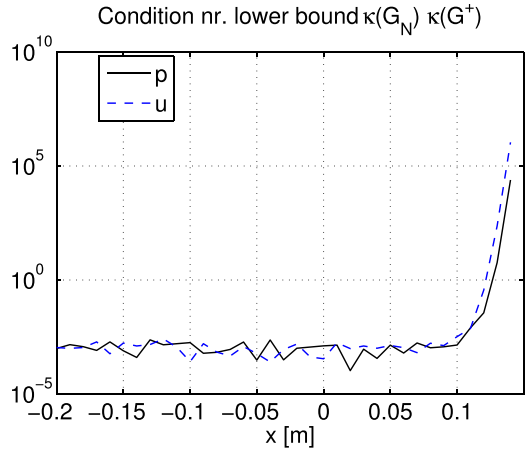

FIG. 14. (Color online) Condition number of the reconstruction matrix for the estimated sound pressure $\mathbf{G}_N(\mathbf{G})^+$ and particle velocity $\mathbf{G}_N(\mathbf{G}_u)^+$.

where κ represents the condition number of the matrix, and the superscript $^+$ the pseudoinverse. This follows from $\kappa(\mathbf{G}_N\mathbf{G}^+) = \|\mathbf{G}_N\mathbf{G}^+\| \cdot \|(\mathbf{G}_N\mathbf{G}^+)^{-1}\| \leq \|\mathbf{G}_N\| \cdot \|\mathbf{G}^+\| \cdot \|(\mathbf{G}_N)^{-1}\| \cdot \|(\mathbf{G}^+)^{-1}\| = \kappa(\mathbf{G}_N)\kappa(\mathbf{G}^+)$. This bound on the condition number of the reconstruction, shown in Fig. 14, demonstrates that the problem is only ill-conditioned when reconstructing closer to the source than the measurement surface. These results are in agreement with the ones shown in Fig. 7 as the reconstruction is closer to—or further from—the source. It is also interesting to note that the error of the sound pressure reconstruction is lower than that of the particle velocity for $x > 0$ (closer to the source): this is because the regularization of the system relies on the sound pressure data, rather than the particle velocity. It is possible to precondition the problem to compensate for the gradient introduced by the particle velocity in the solution, to reduce the ill-conditioning of the full reconstruction problem and obtain a more accurate estimate of the particle velocity and sound intensity.

[1]H. Teutsch and W. Kellermann, "Acoustic source detection and localization based on wavefield decomposition using circular microphone arrays," J. Acoust. Soc. Am. **120**, 2724–2736 (2006).
[2]E. Tiana-Roig, F. Jacobsen, and E. F. Grande, "Beamforming with a circular microphone array for localization of environmental noise sources," J. Acoust. Soc. Am. **128**, 3535–3542 (2010).
[3]E. Tiana-Roig, F. Jacobsen, and E. Fernandez-Grande, "Beamforming with a circular array of microphones mounted on a rigid sphere (L)," J. Acoust. Soc. Am **130**, 1095–1098 (2011).
[4]Y. T. Cho and J. S. Bolton, "Source visualization by using statistically optimized near-field acoustical holography in cylindrical coordinates," J. Acoust. Soc. Am **118**, 2355–2364 (2005).
[5]J. Meyer and G. Elko, "A highly scalable spherical microphone array based on an orthonormal decomposition of the soundfield," in *IEEE International Conference on Acoustics, Speech, and Signal Processing (ICASSP)*, Vol. 2, pp. II-1781–II-1784 (2002).
[6]B. Rafaely, "Plane-wave decomposition of the sound field on a sphere by spherical convolution," J. Acoust. Soc. Am **116**, 2149–2157 (2004).
[7]B. Rafaely, "Analysis and design of spherical microphone arrays," IEEE Trans. Speech Audio Process. **13**, 135–143 (2005).
[8]A. Parthy, C. Jin, and A. van Schaik, "Acoustic holography with a concentric rigid and open spherical microphone array," in *IEEE International Conference on Acoustics, Speech and Signal Processing* (*ICASSP*), 2009, pp. 2173–2176.
[9]Z. Tan, Y. C. Eldar, and A. Nehorai, "Direction of arrival estimation using co-prime arrays: A super resolution viewpoint," IEEE Trans. Signal Process. **62**(21), 5565–5576 (2014).

[10]E. Fernandez-Grande, F. Jacobsen, and Q. Leclere, "Sound field separation with sound pressure and particle velocity measurements," J. Acoust. Soc. Am. **132**, 3818–3825 (2012).
[11]J. Hald, "Patch holography in cabin environments using a two-layer hand held array with an extended SONAH algorithm," in *Proceedings of Euronoise*, Tampere, Finland (2006).
[12]K. Haddad and J. Hald, "3D localization of acoustic sources with a spherical array," J. Acoust. Soc. Am. **123**, 3311 (2008).
[13]A. Pereira and Q. Leclere, "Improving the equivalent source method for noise source identification in enclosed spaces," in *Proceedings of ICSV 18*, Rio de Janeiro, Brazil (July 10–14, 2011).
[14]E. Fernandez-Grande and A. Xenaki, "Compressive sensing with a spherical microphone array," J. Acoust. Soc. Am. **139**(2), EL45–EL49 (2016).
[15]T. Abhayapala and D. B. Ward, "Theory and design of high order sound field microphones using spherical microphone array," in *IEEE International Conference on Acoustics, Speech, and Signal Processing (ICASSP)*, Vol. 2, pp. II-1949–II-1952 (2002).
[16]S. Bertet, J. Daniel, and S. Moreau, "3d sound field recording with higher order ambisonics objective measurements and validation of spherical microphone," in *Audio Engineering Society Convention* (2006).
[17]M. Marschall, S. E. Favrot, and J. Buchholz, "Robustness of a Mixed-Order Ambisonics Microphone Array for Sound Field Reproduction," in *132nd Audio Engineering Society Convention*, Budapest, Hungary (2012).
[18]M. Marschall and J. Chang, "Sound-field reconstruction performance of a mixed-order ambisonics microphone array," Proc. Meet. Acoust. **19**, 055007 (2013).
[19]E. Williams, N. Valdivia, and P. C. Herdic, "Volumetric acoustic vector intensity imager," J. Acoust. Soc. Am. **120**, 1887–1897 (2006).
[20]E. Williams and K. Takashima, "Vector intensity reconstructions in a volume surrounding a rigid spherical microphone array," J. Acoust. Soc. Am. **127**, 773–783 (2010).
[21]F. Jacobsen, G. Moreno-Pescador, E. Fernandez-Grande, and J. Hald, "Near field acoustic holography with microphones on a rigid sphere (L)," J. Acoust. Soc. Am. **129**, 3461–3464 (2011).
[22]A. Granados, F. Jacobsen, and E. Fernandez-Grande, "Regularised reconstruction of sound fields with a spherical microphone array," Proc. Meet. Acoust. **19**, 055010 (2013).
[23]F. Jacobsen, J. Hald, E. Fernandez-Grande, and G. Moreno, "Spherical near field acoustic holography with microphones on a rigid sphere," J. Acoust. Soc. Am. **123**, 3385 (2008).
[24]E. Williams and K. Takashima, "Vector intensity reconstructions in a volume surrounding a rigid spherical measurement array," J. Acoust. Soc. Am. **123**, 3309 (2008).
[25]E. Fernandez-Grande, "Reconstruction of arbitrary sound fields with a rigid-sphere microphone array," in *166th Acoustical Society of America Meeting*, San Francisco, CA (December 2–6, 2013).
[26]E. Fernandez-Grande and T. Walton, "Reconstruction of sound fields with a spherical microphone array," in *Proceedings of Inter-noise 2014*, Melbourne, Australia.
[27]N. P. Vekua, "On the completeness of the system of metaharmonic functions," Dokl. Akad. Nauk SSSR **90**, 715–718 (1953) (in Russian).
[28]G. H. Koopmann, L. Song, and J. B. Fahnline, "A method for computing acoustic fields based on the principle of wave superposition," J. Acoust. Soc. Am **86**, 2433–2438 (1989).
[29]A. Sarkissian, "Method of superposition applied to patch near-field acoustic holography," J. Acoust. Soc. Am **118**, 671–678 (2005).
[30]E. G. Williams, *Fourier Acoustics—Sound Radiation and Nearfield Acoustic Holography* (Academic Press, San Diego, CA, 1999), Chaps. 6 and 8.
[31]J. W. Strutt, "Investigation of the disturbance produced by a spherical obstacle on the waves of sound," Proc. London Math. Soc. **s1–4**(1), 253–283 (1871).
[32]D. L. Sengupta, *Electromagnetic and Acoustic Scattering by Simple Shapes*, edited by J. J. Bowman, T. B. A. Senior, and P. L. E. Uslenghi (Hemisphere, New York, 1987), Chap. 10, Eq. 10.67.
[33]P. C. Hansen, *Rank-Deficient and Discrete Ill-Posed Problems: Numerical Aspects of Linear Inversion*, SIAM monographs on mathematical modeling and computation (SIAM, 1998).
[34]M. Elad, *Sparse and Redundant Representations: From Theory to Applications in Signal and Image Processing* (Springer, New York, 2010), Chap. 1.